Journal of Theoretical and Applied Physics (2020) 14:195–202
https://doi.org/10.1007/s40094-020-00385-2

RESEARCH

The effect of mixed electric field on characteristic of ozone generation in a DBD plasma source

Pourya Seyfi[1] · Mehrdad Rezaei Golghand[1] · Saeed Ghasemi[1] · Hamid Ghomi[1]

Received: 15 June 2020 / Accepted: 6 July 2020 / Published online: 19 July 2020

Abstract

In this paper, we have presented a new power supply structure for ozone generation in a dielectric barrier discharge reactor, so that a high-frequency pulse electric field is applied on the reactor simultaneously with a low-frequency sinusoidal electric field, referred as mixed electric field. In this study, the effect of mixed electric field variation on ozone production efficiency has been investigated and increasing effects on ozone production have been observed when the reactor temperature decreases. This performance has been achieved by modifying the mechanism of electrical discharge and decrease in filamentary discharge in plasma. By examining the spectral lines of atomic emission spectroscopy, the highest peak of the oxygen (O I) spectral lines was observed in the spectrum of the mixed electric field structure. Also by qualitative comparison of the spectral lines, the lowest intensity for the oxygen (O II) spectral lines was observed in this spectrum. Practically, this technique allows us to achieve higher ozone efficiency with less electrical power. Eventually, with the electric field mixing, we were able to achieve a 4.5% efficiency with 7.7 g/h of ozone generation at 2 kW/m^2 with 2 L/min injector oxygen. In addition, by electric field mixing, we were able to reduce the reactor temperature from 66 to 41 °C.

Keywords Ozone generation · DBD · Mixed electric field · Power supply · Electrical discharge · Reactor temperature

Introduction

In recent decades, ozone has been increasingly important between researchers and industries due to its high oxidation potential and applications in many industrial, biological and medical fields [1–4]. This excellent oxidant with advanced oxidation processes is a very strong sterilizer and by participating in chemical reactions in different environments, it can have a variety of applications, including disinfecting water and air purifiers for public environments and hospitals, removing NOX gas from industrial plant outlets, food industries and removing viruses in the medical industry [5–7]. Generally, ozone is generated by an electric discharge in a dielectric barrier discharge (DBD) reactor [8–11]. By applying high voltage in the form of different pulses to the reactor with oxygen gas inlet, ozone is obtained at different concentrations in the outlet [12, 13]. Different applications of ozone require different concentrations of this gas, and different techniques are needed to optimize the systems to increase efficiency [14, 15]. Increasing the reactor temperature is the most important factor in reducing ozone efficiency, which causes a nonlinear reduction in the ozone output [16–18]. Researchers use a variety of techniques to reduce the temperature of the reactor [17, 19–21].

Firstly, the simplest way is to use water-cooling and air-cooling systems which can have a great impact on controlling the reactor temperature and maintaining the ozone production efficiency [22–24]. But to solve this problem fundamentally, we need to find the main factor in increasing the temperature of the reactor. Researchers have investigated the efficiency of ozone production by applying different pulse-shaped power supplies, and by comparing the thermal effects of applying these pulses, the relationships governing the behavior of different power sources on efficiency have extracted. Parameters such as frequency, bipolarity or unipolarity, rise time, duty cycle and electrical power of pulse are the variables that have been the focus of these studies [24–28]. Recent researches have focused on applying nanosecond pulsed power supplies [20, 29]. By examining and comparing the results of these investigations, we conclude that researchers are trying to minimize the thermal

✉ Hamid Ghomi
h-gmdashty@sbu.ac.ir

[1] Laser and Plasma Research Institute, Shahid Beheshti University, Evin, Tehran 1983963113, Iran

effects of the reactor by reducing the pulse width and using nanosecond pulses [20, 29, 30]. In nanosecond pulses, the filamentary discharge does not occur since the pulse time is very low [31–33]. Filamentary discharge is the main cause of increasing the surface temperature of the dielectric [34–36]. We are looking for a way to create a plasma that behaves similarly to plasma generated by nanosecond pulses in a DBD reactor using microsecond and millisecond pulses. Hence, we combine these two pulses and apply them to the reactor simultaneously. The purpose of this configuration of the power supplies is to achieve a uniform plasma to avoid filamentary electrical discharge and reduce the thermal effects of micro-discharges on the dielectric and internal electrode. Finally, by varying the electrical power in each configuration, we identify the highest ozone generation efficiency and introduce the optimal electrical power in millisecond, microsecond and combined electric pulses. In the following, the identification of the species present in the reactor exhaust gas is carried out by optical emission spectrometer (OES). Spectroscopic results play an important role in understanding the performance of factors that increase and decrease ozone output. By comparing qualitatively all of these results, one can have a more accurate answer to the performance of the mixed electric field for ozone generation. Finally, we note that ozone production systems, which use water-cooling systems as well as nanoseconds pulse power supplies to keep the reactor cool, achieve a high efficiency of ozone production. However, the high cost of maintaining water-cooling systems and the lack of nanosecond pulse power supplies in industrial ozone production systems due to its high price have been the reason for the main idea of this article to increase the efficiency of ozone production.

Experimental setup

The experimental setup is shown in Fig. 1. The dielectric barrier discharge plasma is generated in an axially symmetrical electrode configuration, with 5 mm electric discharge gap. The inner electrode is a rod with a diameter of 1 cm. The inner electrode is a steel rod with a diameter of 1 cm and the outer electrode is an aluminum plate with a width of 2 cm and a thickness of 1 mm covering the dielectric tube. The dielectric used is a quartz tube with an outer diameter of 2.2 cm and an inner diameter of 2 cm. Two PTFE holders at the two ends of the reactor have fixed the quartz tube. The location of high-voltage (HV) rod electrode and HV ring electrode as well as current and HV probes are marked in Fig. 1. The outer electrode is connected to a 50 Hz sinusoidal power supply and the other electrode inside the tube is connected to a 6 kHz pulse power supply, as shown in Fig. 1. In all experiments, the inner electrode is driven by a power source, capable of generating a fixed amplitude and duty cycle of pulsed high voltage at 6 kHz frequency, for which the current and voltage waveforms are shown in Fig. 2. On the other hand, the outer electrode is driven by 50 Hz sinusoidal power supply, which is capable of generating a variable high voltage with sinusoidal amplitude (Fig. 3). However, the performance of the mentioned test structure is compared with the other two operating structures, i.e., using both power supply separately to produce ozone gas. The mass flow controller is employed to provide constant O_2 flow (99.99%), which located in the path of the oxygen bottle and the gas inlet of the DBD system. Besides, the oxygen gas flow rate is 2 L/min in all measurements. Electrical discharge in plasma is recorded by a Casio high-speed Exilim Ex-ZR700 Digital Camera. The voltage and the current are measured by a high-voltage probe (TEKTRONIX P6015 1:1000) and a current probe (TCP202 TEKTRONIX), respectively. The electrical signals are visualized using a TEKTRONIX TDS 2024B oscilloscope (200 MHz). The optical emission spectrometer (OES) with model HR 2000 was used to detect the species in plasma. The temperature distribution on the reactor was measured by Fluke VT04A Visual IR Thermometer. The ozone output of the reactor is measured by a BMT 964 UV ozone monitor device. The following equations are used to calculate the average electrical power applied on the plasma DBD.

$$P(t) = V(t) \times I(t) \tag{1}$$

$$E_{\text{pulse}} = \int_0^T P(t)\mathrm{d}t \tag{2}$$

$$P_{\text{ave}} = \frac{E_{\text{pulse}}}{T} \tag{3}$$

where P_{ave} and $P(t)$ are the average and time-dependent electrical power, respectively, E_{pulse} is the energy per pulse, $V(t)$ and $I(t)$ are the time-dependent voltage and current, respectively.

$$P_{\text{TOTAL}} = P_{\text{ave}}(6\ \text{KHz}) + P_{\text{ave}}(50\ \text{Hz}). \tag{4}$$

The total power consumption of two power supplies is shown by P_{TOTAL}.

Results and discussion

The voltage and current waveform generated by the mixed electric field applied on the reactor are shown in Fig. 4. So-called waves-waving-waves can also be attributed to this mixed electric field.

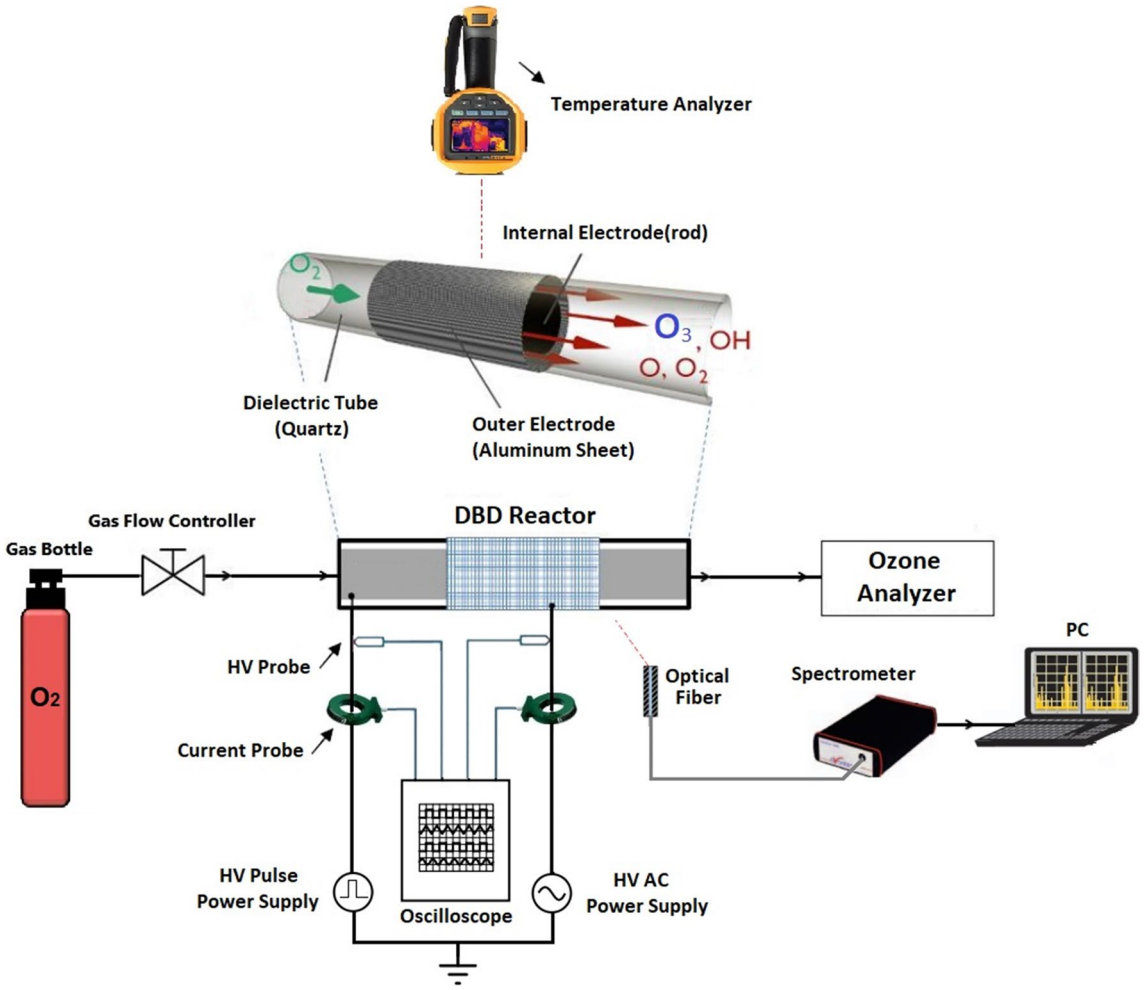

Fig. 1 The schematic of the experimental setup and measurement tools

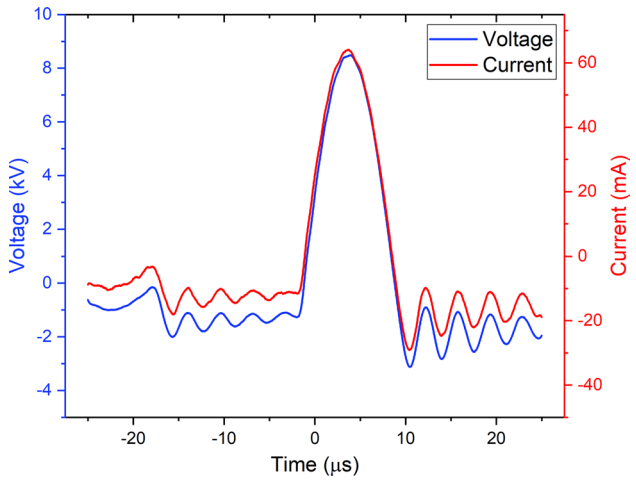

Fig. 2 The voltage and plasma current waveforms of 6 kHz pulsed power supply used for the internal rod electrode

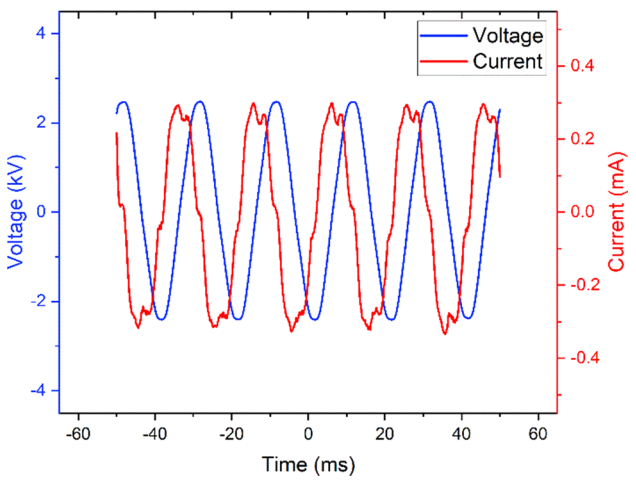

Fig. 3 The voltage and plasma current waveforms of 50 Hz sinusoidal power supply used for the outer electrode

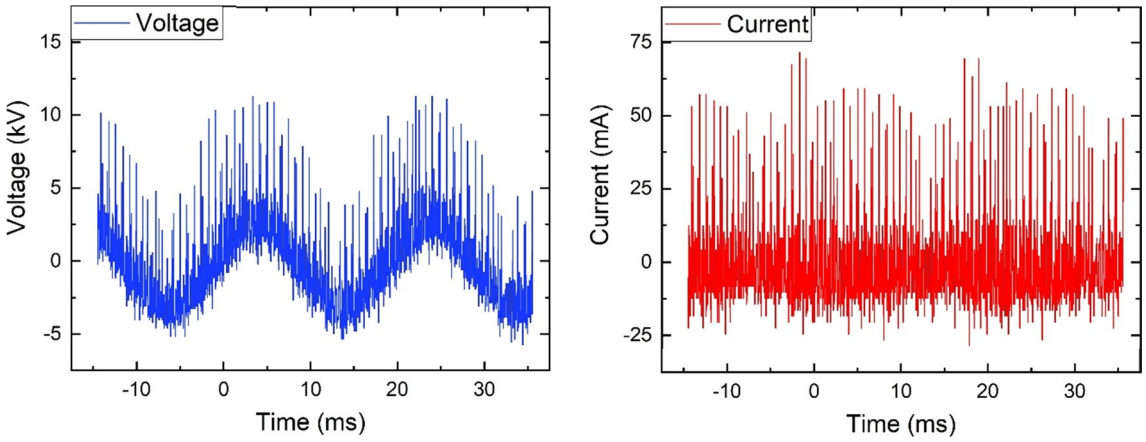

Fig. 4 The voltage and plasma current waveforms when both power supplies are applied simultaneously (amplitude-modulated power supply)

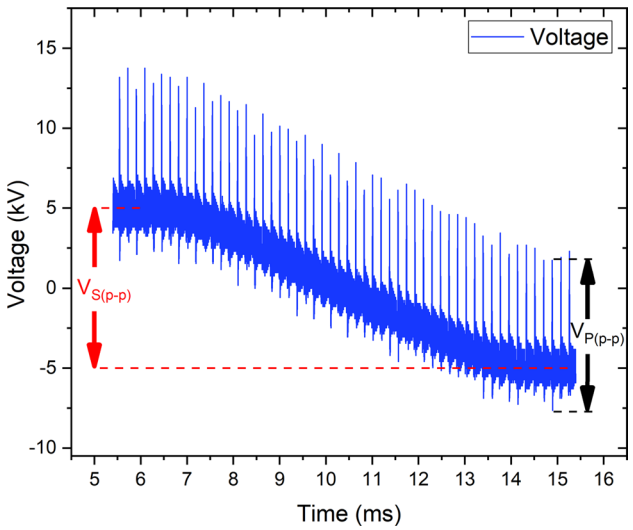

Fig. 5 The modulated voltage amplitude seen on the internal electrode, where the peak-to-peak amplitude of the sinusoidal voltage is Vs(p_p) and the peak-to-peak amplitude of the pulsed voltage is Vp(p_p)

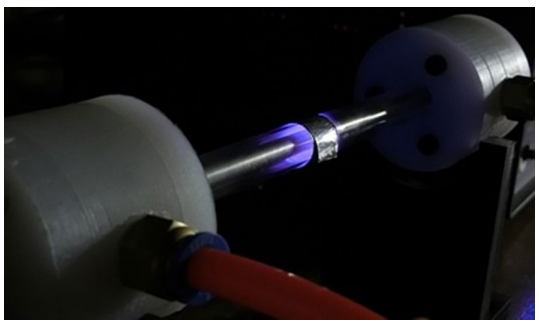

Fig. 6 Photograph of DBD plasma reactor under test stimulated by a mixed electric field

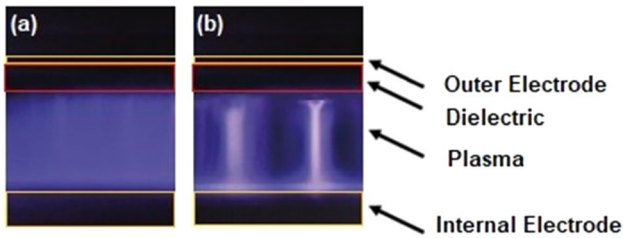

Fig. 7 Photograph of plasma discharge in reactor in power supply mode, **a** mixed electric field and **b** pulsed power supply

As can be seen in the voltage waveform, pulses with a frequency of 6 kHz are modulated on the sinusoidal amplitude of 50 Hz. The modulation of the voltage domain is clearly seen in Fig. 5.

The waveform of the mixed electric field actually represented the electric field of the actuator and the electric discharge current in the plasma. Figure 6 shows a photograph of the discharge structure of a plasma DBD in which oxygen gas is injected and a mixed electric field is applied to it. The plasma is ignited at the gas gap of this reactor. A accurate photograph of the mixed electric field plasma can be seen in Fig. 7a. Also, the reactor is ignited at another stage with the pulse power source. The plasma photograph in this mode is shown in Fig. 7b. By comparing the plasma photograph, the main difference between electric discharge in these two modes is determined. In pulsed plasma mode, plasma filamentary is clearly seen in the electric discharge. But plasma in the mixed electric field mode has no continuous plasma filaments in the electric discharge. Plasma filaments occur randomly in this mode, but are not considered features of this plasma. This performance can be due to the control of the surface electric charge on the dielectric [37, 38]; this control occurs by applying a low-frequency electric field to the dielectric surface [39–41]. Simultaneously,

the high-frequency electric field is applied on the internal electrode by the pulse power supply. The mixed electric field and its results are due to the combination of the effects of the high frequency electric field on the generated plasma and the effects of the low frequency electric field on the dielectric surface. In the next step, this plasma was used to produce ozone and the performance of this structure was compared with other modes. The result of this performance is shown in Fig. 8.

Examining these graphs, we concluded that at low frequencies, although the reactor temperature is lower than other modes, in this frequency range the ozone production rate is generally low. This behavior can be due to the low frequency of the electric field applied on oxygen molecules. By applying pulse power supply, we have seen an increase in ozone production efficiency. By applying a pulsed power supply, we have seen an increase in the efficiency of ozone production, but with increasing efficiency, the reactor temperature also rises sharply and causing a sharp decrease in efficiency. In the structure of the mixed electric field, the enhancing of ozone production efficiency was observed; also, in this mode, the temperature control of the reactor was done well. The efficiency of ozone production with reverse bias in the mixed electric field mode decreases sharply. This performance is due to the high temperature of the reactor. The nonlinear increase in reactor temperature in this mode can be due to the thermal effects of the electrical discharge in the reactor. The thermal effects of the reactor in this mode can be due to the increase in plasma filaments in the electrical discharge. The final comparison of the graphs is shown in Fig. 9.

Comparing the graphs in Fig. 9, we conclude that we had the lowest ozone production rate at 50 Hz. Optimal power in this mode is lower than other modes. In pulse mode, we have an increase in ozone efficiency compared to the previous mode. In this mode, the optimal electrical power is greatly increased. In mixed electric field mode, we achieved a higher efficiency than other modes. In this mode, we achieve this efficiency at a lower optimum power. From the obtained graphs, the strong dependence of ozone production on reactor temperature is observed. From the atomic-molecular point of view, the mechanism of reactor performance in

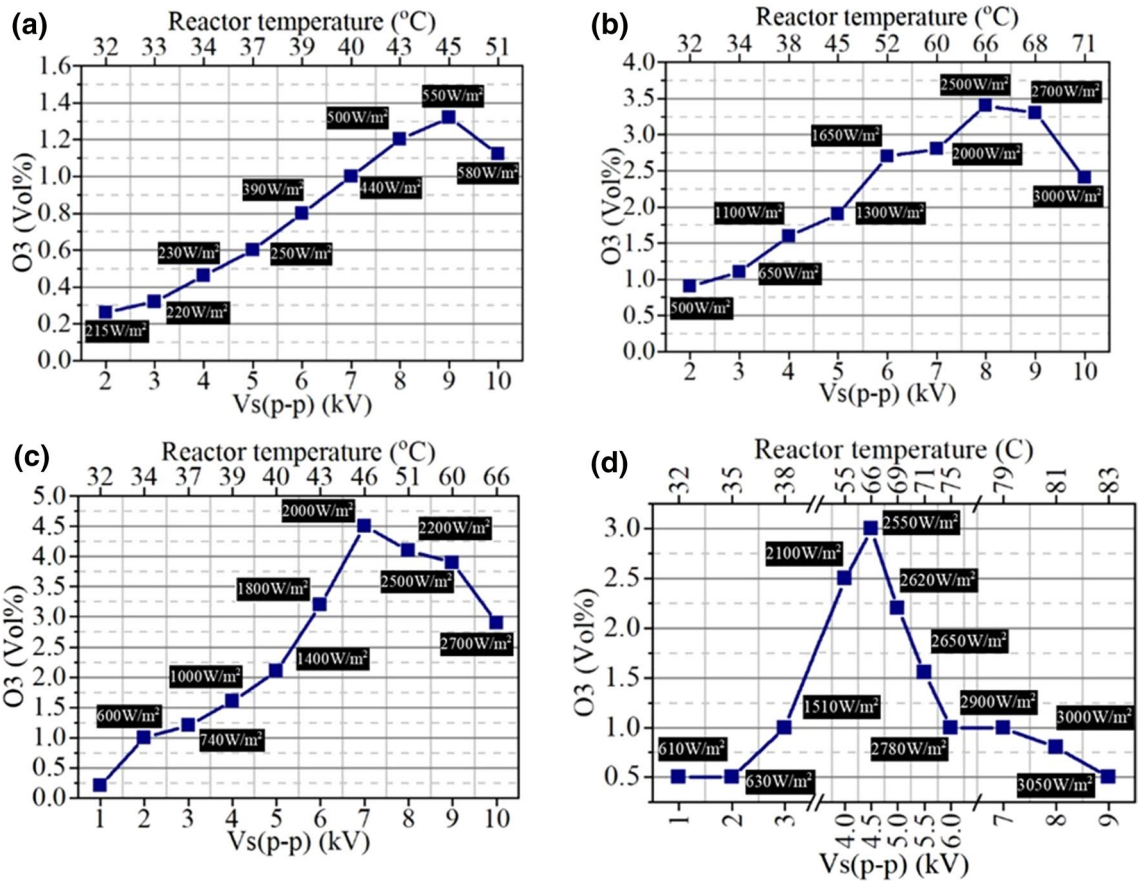

Fig. 8 Graph of variation in ozone production efficiency and reactor temperature by varying the voltage and power applied on the reactor in four different operating modes: apply power supply **a** 50 Hz (AC), **b** 6 kHz (pulsed), **c** mixed electric field and **d** mixed electric field (by inverting power supplies)

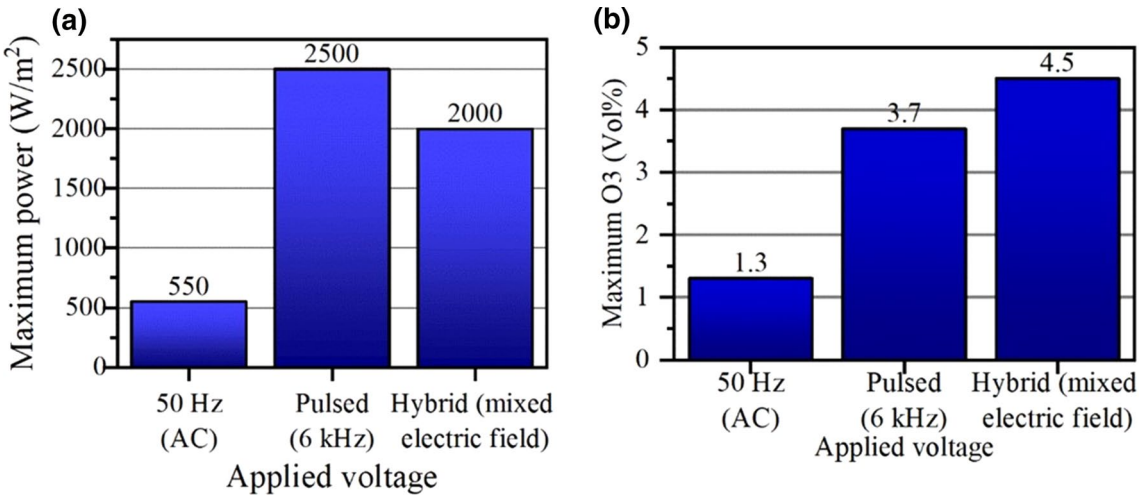

Fig. 9 The final results of the ozone output efficiency of the reactor and their comparison, **a** optimal power for different conditions and **b** maximum ozone efficiency of reactor output for optimum power

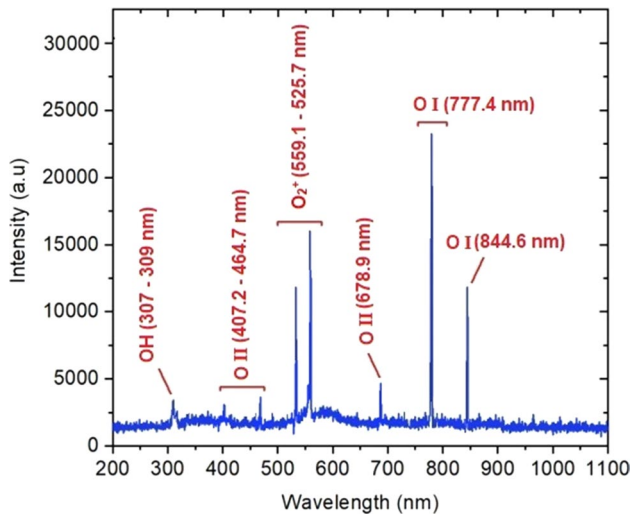

Fig. 10 The OES of plasma driven by mixed electric field mode at 1 cm away from the dielectric tube

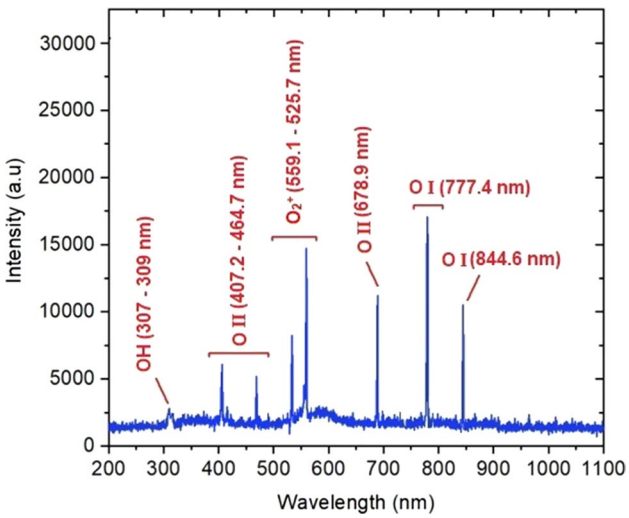

Fig. 11 The OES of plasma driven by pulsed power supply mode at 1 cm away from the dielectric tube

different modes has been investigated by spectroscopy and spectral lines in Figs. 10, 11 and 12. In spectral lines, the OH molecular spectrum, oxygen spectral lines (O I and O II) and the molecular spectrum of oxygen (O_2^+) are observed. These spectral lines and their transition lines are shown in Table 1. The intensity of O I oxygen lines indicates the possibility of ozone production. Also, the intensity of the O II oxygen lines indicates the possibility of ozone recombination. By observing these spectral lines, we can see that in mixed electric field mode, we have the highest intensity of O I oxygen spectral lines. In this mode, the intensity of the O II oxygen spectral lines is lower level. O II oxygen spectral lines related to pulse power supply mode are at the highest level.

Conclusion

In this study, we investigated the rate of ozone generation by the ratio of inlet oxygen in a DBD reactor driven by a mixed electric field. The internal electrode of the reactor was driven by a high-voltage high-frequency pulsed power supply with constant output voltage and simultaneously the outer electrode was biased by the high-voltage low-frequency sinusoidal power supply with variable output voltage. It was observed that by increasing the bias voltage and subsequently increasing the power applied on the reactor, the temperature of the reactor also increases linearly. But the increasing trend of the temperature in different power

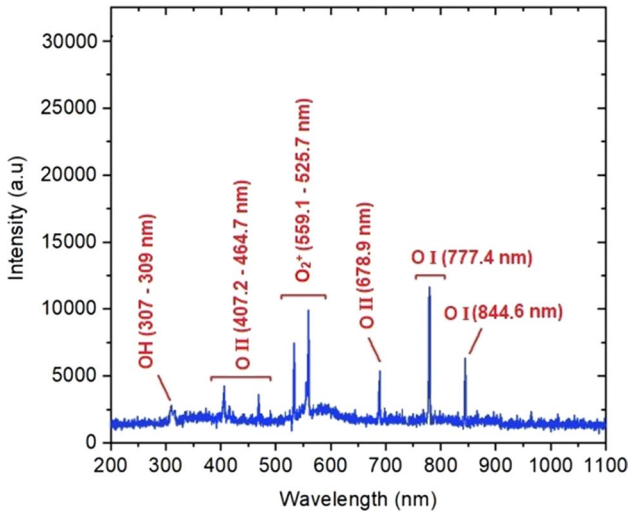

Fig. 12 The OES of plasma driven by 50 Hz (AC) power supply mode at 1 cm away from the dielectric tube

Table 1 Main spectral lines observed in OES of reactor plasma

Oxygen species	Transition line	Wavelength (nm)
O (O I)	$3p^5P \rightarrow 3s^5S$	777.4
	$3p^3P \rightarrow 3s^3S$	844.6
O_2^+	$b_4 \sum_g \rightarrow a_4 \prod u$	559.1
	$b_4 \sum_g \rightarrow a_4 \prod u$	525.7
O^+ (O II)	–	678.9
	$3p^4D \rightarrow 3s^4P$	464.7
	$3d^4F \rightarrow 3p^4D$	407.2

supply structures was different. As the reactor temperature increases, the ozone production efficiency also increases, but this increase in each structure stops at a certain power. A sharp increase in reactor temperature after this power and saturation of ozone production results in nonlinear behavior in efficiency and a sharp decrease in ozone production. Our proposed structure results in increased ozone production efficiency by lowering temperature and reducing power consumption compared to the structures investigated in this study. This observation would be due to the decrease in the thermal effects of plasma filamentary by electrical discharge on dielectrics and internal electrode. In fact, low-frequency biasing controls the amount of charge accumulated on the dielectric surface and subsequently the type of plasma discharge and plasma regime in the reactor which results reducing the reactor temperature from 66 to 41 °C relative to the pulsed structure. As a result, despite low energy consumption, we had a 0.8 percent increase in ozone production efficiency. From the spectroscopic point of view of spectral species in reactor gas, we can conclude that in the structure of the mixed electric field, O I oxygen spectral lines are much qualitatively stronger than O II oxygen lines. Increasing the range of O I oxygen peaks can be an important factor in increasing the likelihood of ozone molecule bond formation. In this spectral range, the reduction of the O II oxygen spectrum can be a reason for the reduction of ozone molecule recombination. The behavior of spectral species indicates that the bias structure of the power source for ozone production is optimized by the combined electric field structure.

References

1. Yamamoto, H., et al.: Pilot-scale NO_x and SO_x aftertreatment using a two-phase ozone and chemical injection in glass-melting-furnace exhaust gas. IEEE Trans. Ind. Appl. **55**(6), 6295–6302 (2019)
2. Alves Filho, E., et al.: An untargeted chemometric evaluation of plasma and ozone processing effect on volatile compounds in orange juice. Innov. Food Sci. Emerg. Technol. **53**, 63–69 (2019)
3. Crema, A.P.S., et al.: Degradation of indigo carmine in water induced by non-thermal plasma, ozone and hydrogen peroxide: a comparative study and by-product identification. Chemosphere **244**, 125502 (2020)
4. Madhukar, A., Rajanikanth, B.: Cascaded plasma-ozone injection system: a novel approach for controlling total hydrocarbon emission in diesel exhaust. Plasma Chem. Plasma Process. **39**(4), 845–862 (2019)
5. Abdelaziz, A.A., et al.: Quantitative analysis of ozone and nitrogen oxides produced by a low power miniaturized surface dielectric barrier discharge: effect of oxygen content and humidity level. Plasma Chem. Plasma Process. **39**(1), 165–185 (2019)
6. Fan, R., et al.: Effect of the reaction temperature on the removal of diesel particulate matter by ozone injection. Plasma Chem. Plasma Process. **39**(1), 143–163 (2019)
7. Yamasaki, H., et al.: Plasma-chemical hybrid NO_x removal in flue gas from semiconductor manufacturing industries using a blade-dielectric barrier-type plasma reactor. Energies **12**(14), 2717 (2019)
8. Kuvshinov, D., et al.: Efficient compact micro DBD plasma reactor for ozone generation for industrial application in liquid and gas phase systems. Int. J. Chem. Mol. Nucl. Mater. Metall. Eng. **8**(1), 80–83 (2020)
9. Nemmich, S., et al.: Experimental analysis of the influence of the voltage waveform on ozone generation efficiency. Int. J. Environ. Stud. **76**(4), 571–581 (2019)
10. Wei, L., Deng, Q., Zhang, Y.: Ozone generation enhanced by silica catalyst in oxygen-fed dielectric barrier discharge. Vacuum **173**, 109145 (2020)
11. Wu, Q., et al.: Current balancing of paralleled SiC MOSFETs for a resonant pulsed power converter. IEEE Trans. Power Electron. **35**, 5557–5561 (2019)
12. Samaranayake, W., et al.: Pulsed streamer discharge characteristics of ozone production in dry air. IEEE Trans. Dielectr. Electr. Insul. **7**(2), 254–260 (2000)
13. Wei, L., Xu, M., Zhang, Y.: Energy conversion and temperature dependence in ozone generator using pulsed discharge in oxygen. Ozone Sci. Eng. **39**(1), 33–43 (2017)
14. Selma, M.V., et al.: Disinfection potential of ozone, ultraviolet-C and their combination in wash water for the fresh-cut vegetable industry. Food Microbiol. **25**(6), 809–814 (2008)

15. Pavlovich, M.J., et al.: Ozone correlates with antibacterial effects from indirect air dielectric barrier discharge treatment of water. J. Phys. D Appl. Phys. **46**(14), 145202 (2013)
16. Jodzis, S., Barczyński, T.: Ozone synthesis and decomposition in oxygen-fed pulsed DBD system: effect of ozone concentration, power density, and residence time. Ozone Sci. Eng. **41**(1), 69–79 (2019)
17. Zhang, Y., et al.: Ozone production in coaxial DBD using an amplitude-modulated AC power supply in air. Ozone Sci. Eng. **41**(5), 437–447 (2019)
18. Baloul, Y., et al.: Experimental assessment of ozone production by multichannel plasma discharges for automotive applications. J. Phys. D Appl. Phys. **52**(27), 275204 (2019)
19. Alhamid, M.I., et al.: Performance analysis and water quality after ozone application in closed circuit cooling tower systems. In: AIP Conference Proceedings. AIP Publishing LLC (2019)
20. Hidaka, H., et al.: Characteristics of nanosecond pulsed discharge type ozonizer with a tube to cylinder reactor. In: 2019 IEEE Pulsed Power and Plasma Science (PPPS). IEEE (2019)
21. Sanuki, Y., et al.: Investigation of energy control in coaxial reactor for ozone production by using nanosecond pulsed power. In: 2019 IEEE Pulsed Power and Plasma Science (PPPS). IEEE (2019)
22. Ohta, K., Wada, N., Kuzumoto, M.: Characteristics of ozone generation by both electrodes cooling ozone generator. IEEJ Trans. Fundam. Mater. **120**(6), 695–700 (2000)
23. Jodpimai, S., Boonduang, S., Limsuwan, P.: Dielectric barrier discharge ozone generator using aluminum granules electrodes. J. Electrostat. **74**, 108–114 (2015)
24. Park, S.-L., et al.: Effective ozone generation utilizing a meshed-plate electrode in a dielectric-barrier discharge type ozone generator. J. Electrostat. **64**(5), 275–282 (2006)
25. Chen, J., Davidson, J.H.: Ozone production in the negative DC corona: the dependence of discharge polarity. Plasma Chem. Plasma Process. **23**(3), 501–518 (2003)
26. Šimek, M., Pekárek, S., Prukner, V.: Ozone production using a power modulated surface dielectric barrier discharge in dry synthetic air. Plasma Chem. Plasma Process. **32**(4), 743–754 (2012)
27. Šimek, M., Pekárek, S., Prukner, V.: Influence of power modulation on ozone production using an AC surface dielectric barrier discharge in oxygen. Plasma Chem. Plasma Process. **30**(5), 607–617 (2010)
28. Hong, D., et al.: Measurement of ozone production in non-thermal plasma actuator using surface dielectric barrier discharge. Plasma Chem. Plasma Process. **34**(4), 887–897 (2014)
29. Fukuoka, H., et al.: Improvement of ozone generation characteristics with shorter rise time of nanosecond pulse voltage. In: 2019 IEEE Pulsed Power and Plasma Science (PPPS). IEEE (2019)
30. Matsukawa, R., et al.: Development of a compact nanosecond pulse generator. In: 2019 IEEE Pulsed Power and Plasma Science (PPPS). IEEE (2019)
31. Ryu, T., Wang, D., Namihira, T.: Behavioral characteristics of nanosecond pulsed discharge in coaxial electrodes. Electr. Eng. Jpn. **210**, 19–28 (2020)
32. Wang, D., Namihira, T.: Nanosecond pulsed streamer discharges: II. Physics, discharge characterization and plasma processing. Plasma Sources Sci. Technol. **29**(2), 023001 (2020)
33. Yamaguchi, H., et al.: Observation of positive and negative nanosecond pulsed streamers in a coaxial electrode using a quadruple emICCD camera system. In: 2019 IEEE Pulsed Power and Plasma Science (PPPS). IEEE (2019)
34. Kong, C., et al.: Stabilization of a turbulent premixed flame by a plasma filament. Combust. Flame **208**, 79–85 (2019)
35. Wang, Q., et al.: Characteristics and mechanisms of transition from filament to homogeneous glow in atmospheric helium dielectric barrier discharges under variation of the applied voltage amplitude. J. Phys. D Appl. Phys. **52**(20), 205201 (2019)
36. Ding, C., et al.: Streamer-to-filamentary transition and electron temperature measurement in positive polarity nanosecond surface discharge between 1 and 10 bar. In: AIAA Scitech 2019 Forum (2019)
37. Elias, P., Castera, P.: Measurement of the impulse produced by a pulsed surface discharge actuator in air. J. Phys. D Appl. Phys. **46**(36), 365204 (2013)
38. Eid, A., Takashima, K., Mizuno, A.: Experimental and simulation investigations of DBD plasma reactor at normal environmental conditions. IEEE Trans. Ind. Appl. **50**(6), 4221–4227 (2014)
39. Sato, S., et al.: Successively accelerated ionic wind with integrated dielectric-barrier-discharge plasma actuator for low-voltage operation. Sci. Rep. **9**(1), 1–11 (2019)
40. Truong, H.T., et al.: Effects of dielectric properties on electrical characteristics of dielectric barrier discharge generated by low frequency uni-polar high voltage pulses. Jpn. J. Appl. Phys. **58**(11), 111001 (2019)
41. Yadala, S., et al.: Effect of DBD plasma actuators on vortical structures in a turbulent mixing layer. In: 11th International Symposium on Turbulence and Shear Flow Phenomena, TSFP (2019)